Food and Chemical Toxicology 162 (2022) 112869

Contents lists available at ScienceDirect

Food and Chemical Toxicology

journal homepage: www.elsevier.com/locate/foodchemtox

Imatinib disturbs lysosomal function and morphology and impairs the activity of mTORC1 in human hepatocyte cell lines

Noëmi Johanna Roos [a,b,1], Riccardo Vincenzo Mancuso [a,c,1], Gerda Mawududzi Sanvee [a,b], Jamal Bouitbir [d], Stephan Krähenbühl [a,*]

[a] Division of Clinical Pharmacology & Toxicology, University Hospital of Basel, Switzerland
[b] Division of Pharmaceutical Technology, Department of Pharmaceutical Sciences, University of Basel, Switzerland
[c] Division of Molecular Pharmacy, Department of Pharmaceutical Sciences, University of Basel, Switzerland
[d] Division of Molecular and Systems Toxicology, Department of Pharmaceutical Sciences, University of Basel, Switzerland

ARTICLE INFO

Handling editor. Dr. Jose Luis Domingo

Keywords:
Tyrosine kinase inhibitors (TKI)
Hepatotoxicity
HepG2 cells
mTORC1
TFEB
Autophagy

ABSTRACT

The tyrosine kinase inhibitors (TKIs) imatinib and lapatinib are associated with severe hepatotoxicity, whose mechanisms are currently under investigation. As amphiphilic drugs, imatinib and lapatinib enrich in lysosomes. In the present study, we investigated their effects on lysosomal morphology and function in HepG2 and HuH-7 cells and explored possible links between lysosomal dysfunction and hepatotoxicity. Both TKIs increased the lysosomal volume time and concentration-dependently in HepG2 and HuH-7 cells. In HepG2 cells, lapatinib and imatinib raised the lysosomal pH and destabilized the lysosomal membrane, thereby impairing lysosomal proteolytic activity such as cathepsin B processing. Imatinib activated the transcription factor EB (TFEB), a regulator of lysosomal biogenesis and function, as demonstrated by nuclear TFEB accumulation and increased expression of TFEB-target genes. Because of lysosomal dysfunction, imatinib impaired mTORC1 activation, a protein complex activated on the lysosomal surface, which explained TFEB activation. HepG2 cells treated with imatinib showed increased levels of MAP1LC3A/B-II and of ATG13 (S318) phosphorylation, indicating induction of autophagy due to TFEB activation. Finally, imatinib induced apoptosis in HepG2 cells in a time and concentration-dependent manner, explained by lysosomal and mitochondrial toxicity. Our findings provide a new lysosome-centered mechanism for imatinib-induced hepatotoxicity that could be extended to other lysosomotropic drugs.

1. Introduction

Tyrosine kinases (TKs) are transmembranous or cytosolic proteins that phosphorylate intracellular protein tyrosine residues after having been activated by binding of their ligands. Activated TKs initiate intracellular signaling pathways that regulate fundamental processes such as cell differentiation, proliferation, and apoptosis (Krause and Van Etten, 2005). Permanently activated TKs can lead to uncontrolled cell growth and cancer. Small-molecule drugs that specifically inhibit oncogenic TKs, classified as tyrosine kinase inhibitors (TKIs), are therefore efficacious anticancer drugs (Huang et al., 2020).

Imatinib mesylate, the first approved TKI, inhibits the breakpoint cluster region protein-Abelson tyrosine kinase (BCR-ABL) fusion protein by competitively binding to the ATP-binding site of the protein (Goldman and Melo, 2001). Furthermore, imatinib is an inhibitor of the oncogenic platelet-derived growth factor receptor, stem cell factor, and c-Kit. Imatinib is indicated to treat patients with BCR-ABL positive chronic myelogenous leukemia (CML) and acute lymphoblastic leukemia, gastrointestinal stromal tumors, mastocytosis, and other tumors caused by imatinib-sensitive TK (Peng et al., 2005). The most frequent adverse effects of imatinib are edema, myalgias, and gastrointestinal irritations (Druker et al., 2001). In addition, imatinib is associated with liver injury, which is in most cases asymptomatic and transient (Peng et al., 2005). However, severe cases of liver injury leading to liver transplantation or death have also been reported in patients treated with imatinib (Lin et al., 2003).

Lapatinib, a TKI that inhibits the erb-b2 receptor tyrosine kinase 2 (ERBB2), is approved for the treatment of advanced or metastatic ERBB2-positive breast cancer (Moy et al., 2007). Common adverse

* Corresponding author. Clinical Pharmacology & Toxicology University Hospital, 4031, Basel, Switzerland.
E-mail address: stephan.kraehenbuehl@usb.ch (S. Krähenbühl).
[1] contributed equally to this work.

https://doi.org/10.1016/j.fct.2022.112869
Received 24 October 2021; Received in revised form 20 December 2021; Accepted 12 February 2022
Available online 16 February 2022

List of abbreviations

TKI	Tyrosine kinase inhibitor
TK	Tyrosine kinase
CML	Chronic myelogenous leukemia
LTDR	LysoTracker Deep Red
AO	Acridine orange
DQ-BSA	De-quenched bovine serum albumin
mTOR	Mechanistic target of rapamycin kinase
CTSB	Cathepsin B
TFEB	Transcription factor EB
mTORC1/2	Mechanistic target of rapamycin kinase complex 1/2
AKT1	AKT serine/threonine kinase 1
GSK3B	Glycogen synthase kinase 3 beta
MAPK1/3	Mitogen-activated protein kinase 1/3
ULK1	Unc-51 like autophagy activating kinase 1
RPS6	Ribosomal protein S6
EIF4EBP1	Eukaryotic translation initiation factor 4E binding protein 1
TSC1/2	TSC complex
PRKAA	Protein kinase AMP-activated catalytic subunit alpha 1 and 2
SQSTM1	Sequestosome 1
ATG13	Autophagy related protein 13
MAP1LC3A/B	Microtubule associated protein 1 light chain 3 alpha/beta
LMP	Lysosomal membrane permeabilization

reactions associated with lapatinib include gastrointestinal irritations, rash, palmar-plantar erythrodysesthesia, and fatigue (Ryan et al., 2008). In 2008, the U.S. Food and Drug Administration prompted a black box warning due to severe cases of acute liver toxicity caused by lapatinib, including cases with fatal outcome (Azim et al., 2013).

We have previously reported that imatinib and lapatinib are mitochondrial toxicants, which may partially explain hepatotoxicity associated with these drugs (Paech et al., 2017). In a more recent study, we observed that the hepatotoxic multi-kinase inhibitors ponatinib, regorafenib and sorafenib rapidly increased the number and size of lysosomes in HepG2 cells, a hepatocyte-derived immortalized cell line (Paech et al., 2018). Due to their physicochemical properties (lipophilic compounds with a nitrogen atom that can be protonated), several TKIs including lapatinib and imatinib have been reported to accumulate in lysosomes (Burger et al., 2015; Fu et al., 2014; Nadanaciva et al., 2011). Since lysosomal drug accumulation can disturb the lysosomal function and cause cytotoxicity (Boya et al., 2003a, 2003b), we hypothesized that lysosomal accumulation of TKIs may represent an additional mechanism of hepatotoxicity. Based on these considerations, we decided to study the effect of lapatinib and imatinib on lysosome morphology and function as well as the relation to cytotoxicity in HepG2 cells.

2. Materials and methods

2.1. Reagents

Cell culture media (DMEM, low glucose, pyruvate, 31885023; DPBS, no calcium, no magnesium, 14190094), supplements (fetal bovine serum, 10500064; HEPES, 15630056; GlutaMAX, 35050038; MEM non-essential amino acids solution, 11140035; penicillin-streptomycin 10'000 U/mL, 15140122), and TrypLE express enzyme (12605010) were purchased from Thermo Fisher Scientific. Imatinib mesylate (SRP00530i) and lapatinib (SRP01210l) were obtained from Sequoia Research Products. Bafilomycin A1 (1334) and chloroquine diphosphate (4109) were purchased from Bio-Techne, while amiodarone hydrochloride (A8423), staurosporine (S5921), doxorubicin hydrochloride (D1515), and PIPES (P6757), BSA (A7906) and Tween 20 (93773) were ordered from Sigma-Aldrich. The antibodies were obtained from the companies listed in Table S1. Microsynth produced the primers listed in Table S2. The reagents used for transmission electron microscopy (paraformaldehyde, 15710; glutaraldehyde, 16310; osmium tetroxide, 19100; uranyl acetate, 22400; acetone, 15056; Epon812 resin, 14120) were ordered from Electron Microscopy Sciences.

2.2. Cell culture

HepG2 cells (ATCC, HB-8065), a human hepatoma cell line, were cultured in DMEM (1.0 g/L D-glucose, 4 mM L-glutamine, 1 mM sodium pyruvate) supplemented with 10% (v/v) inactivated FBS, 10 mM HEPES buffer (pH 7.4), 2 mM GlutaMAX, 1% (v/v) MEM non-essential amino acids solution (100x), and 100 U/mL penicillin/streptomycin. We grew the cells in a humidified 5% CO_2 cell culture incubator (Heracell 150i, Thermo Fisher Scientific, Basel, Switzerland) at 37 °C and passaged them using TrypLE express enzyme. We subcultured the cells in a ratio of 1:5 and did not exceed a passage number of 30. Both cell number and cell viability were determined by trypan blue exclusion using the EVE automatic cell counter (NanoEnTek, Seoul, Korea).

HuH-7 cells (RCB1366, RIKEN Cell Bank), a human hepatoma cell line, were cultured at 37 °C in a humidified 5% CO_2 cell culture incubator. The cells were kept in DMEM High Glucose 4.5 g/L (BioConcept, 1–26F03-I) supplemented with 10% fetal bovine serum (Thermo Fisher Scientific, 10500064) and 1% penicillin-streptomycin (10'000 μg/mL; Thermo Fisher Scientific, 15140122). We subcultured the cells in a ratio of 1:5 when they reached 70% confluency and did not exceed a passage number of 30.

2.3. Drug treatment

We treated HepG2 cells (80% confluency) with imatinib mesylate (5–50 μM) and lapatinib (2–20 μM) for 0.5, 6, and 24 h. The drug stock solutions (1'000x) were prepared in DMSO (Sigma-Aldrich, 472301) and stored at -20 °C. The DMSO concentration in the incubations did not exceed 0.1%. Negative control incubations (Ctrl) contained 0.1% (v/v) DMSO in the respective incubation buffer.

2.4. Flow cytometry with LTDR

We assessed the volume of the lysosomal compartment in imatinib- and lapatinib-treated HepG2 cells using LysoTracker Deep Red (LTDR, Thermo Fisher Scientific, L12492). LTDR is a fluorescent dye ($\lambda_{ex./em.}$ = 647⁄668 nm) that accumulates in lysosomes. We seeded HepG2 cells in a 24-well plate (150'000 cells/well) and treated them with imatinib and lapatinib for 0.5 h, 6 h, and 24 h. Amiodarone (50 μM), an amphiphilic drug that enlarges the lysosomal compartment, was used as a positive control (Funk and Krise, 2012). After the treatment, we harvested the cells using TrypLE express enzyme, transferred them into a clear V-bottom 96-well plate (Sigma-Aldrich, CLS3897-100 EA), and pelleted

the cells by centrifugation (400 *g*, 5 min). We resuspended the cell pellet in LTDR solution (1 nM, 200 µL/well) prepared in pre-warmed (37 °C) cell culture medium and incubated for 5 min (37 °C, protected from light). Afterward, the cells were pelleted again by centrifugation (400 *g*, 5 min) and resuspended in pre-warmed (37 °C) cell culture medium. The cells were subsequently analyzed with a CytoFLEX flow cytometer (Beckman Coulter, Indianapolis, IN, USA). For the flow cytometry gating strategy, singlets were first identified by a forward scatter area (FSC-A) and forward scatter height (FSC-H) gate, and then by an FSC-A and side scatter area (SSC-A) gate. The fluorescence of 10'000 HepG2 cells from five independent replicates for each condition was quantified using the FL-5-A channel and analyzed with the FlowJo software (Tree Star, Ashland, OR, USA).

2.5. Fluorescence microscopy with LTDR

We assessed the lysosomal morphology with a fluorescence microscope using LTDR and Hoechst 33342 (Sigma-Aldrich, 14533) as lysosomal and nuclear staining, respectively. In brief, HepG2 cells were grown into a six channel (18'000 cells/channel) ibiTreat µ-Slide VI 0.4 (ibidi, 80606) and treated with imatinib (10 µM) and lapatinib (5 µM) for 24 h. We stained the cells with 100 µL/channel LTDR (100 nM) and Hoechst 33342 (1 µM) dissolved in cell culture medium (1 h, 37 °C, protected from light). Then, we washed and covered the cells with cell culture medium and acquired microscopic pictures with an Olympus IX83 microscope (Olympus, Tokyo, Japan).

2.6. Acridine orange redistribution

We assessed the redistribution of acridine orange (AO) hydrochloride (Bio-Techne, 5092) as a measure of lysosomal pH and stability (Palmgren, 1991). AO exhibits red and green fluorescence when located in acidic compartments (e.g., lysosomes) and cytosol, respectively. An increased ratio of AO green-to-red indicates a loss of lysosomal pH gradient and/or decreased lysosomal stability (Yoshimori et al., 1991). HepG2 cells seeded in a black-walled 96-well plate (25'000 cells/well) were incubated with AO (5 µM) diluted in cell culture medium (15 min, 37 °C, protected from light). Afterward, the cells were washed with medium and treated with imatinib and lapatinib for 6 h or 24 h. As lysosomal pH-raising drugs, bafilomycin A1 (0.1 µM) and chloroquine (30 µM) were used as positive controls (Poole and Ohkuma, 1981; Yoshimori et al., 1991). After the treatment, we covered the cells with PBS and measured the red ($\lambda_{ex./em.}$ = 460⁄650 nm) and green ($\lambda_{ex./em.}$ = 495⁄530 nm) fluorescence using a microplate reader (Infinite 200 PRO, Tecan Group, Männedorf, Switzerland). After the measurement, we lysed the cells with radioimmunoprecipitation (RIPA) buffer (60 µL/well) and determined the protein concentration of each well using the Pierce BCA Protein Assay Kit (Thermo Fisher Scientific, 23225). The fluorescence intensities were normalized to the protein concentration and the ratio green-to-red AO fluorescence was calculated. We run the experiment with at least three independent replicates for each condition.

2.7. Flow cytometry with DQ-BSA

We investigated the lysosomal proteolytic activity of imatinib- and lapatinib-treated HepG2 cells using de-quenched green bovine serum albumin (DQ-BSA, Thermo Fisher Scientific, D12050) (Klionsky et al., 2016; Reis et al., 1998). DQ Green BSA consists of BSA conjugated to self-quenched Bodipy FL dye. After endocytosis and lysosomal accumulation, DQ Green BSA is degraded by lysosomal proteases releasing fluorescent ($\lambda_{ex./em.}$ = 505⁄515 nm) BSA-fragments (Fig. S7). HepG2 cells were seeded in a 24-well plate (150'000 cells/well) and treated with imatinib and lapatinib for 6 h and 24 h. Four hours before the treatment was completed, we pulsed the cells for 2 h with DQ Green BSA (100 µg/mL), which was followed by a 2 h-chase period. Both pulse and chase were conducted in the presence of the drug. Finally, the cells were harvested using TrypLE express enzyme, transferred to a V-bottom 96-well plate, and pelleted by centrifugation (400 *g*, 5 min). We resuspended the cells in pre-warmed (37 °C) cell culture medium and analyze them with the CytoFLEX flow cytometer. Singlets were gated as described above. The fluorescence of 10'000 HepG2 cells was quantified using the FL-1-A channel and analyzed with the FlowJo software. We run the experiment with five independent replicates for each condition.

2.8. Western blotting

Protein expression in imatinib-treated HepG2 cells was assessed by Western blotting as described before (Roos et al., 2020). In brief, we loaded denatured and reduced protein samples (10–20 µg protein) on a NuPage 4–12% Bis-Tris Gel (Thermo Fisher Scientific, NP0335BOX) and ran a one-dimensional gel electrophoresis. We used NuPAGE LDS sample buffer (Thermo Fisher Scientific, NP0007) and PageRuler prestained protein ladder (Thermo Fisher Scientific, 26617) as loading buffer and molecular weight marker, respectively. The separated proteins were transferred on a 0.2 µm nitrocellulose membrane (Bio-Rad, 1620112) using the eBlot L1 transfer sandwich (GenScript, L00724) and wet protein transfer system (GenScript, Piscataway, NJ, USA). The membrane was blocked under constant orbital shaking (1 h, at room temperature) with 5% (w/v) non-fat dried milk or BSA (as recommended by the manufacturer) in PBS containing 0.1% (v/v) Tween 20 (PBST). Subsequently, the membrane was incubated with the primary antibody diluted in 5% (w/v) non-fat dried milk or BSA in PBST under constant shaking (overnight, at 4 °C). To assess the protein phosphorylation, we used PhosphoSafe Extraction Buffer (Merck, 71296) and 5% (w/v) BSA in PBS containing 0.1% (v/v) Tween 20 as blocking buffer. The primary antibodies and dilutions are listed in Table S1. Glyceraldehyde-3-phosphate dehydrogenase (GAPDH) and Lamin B1 served as cytoplasmic and nuclear loading control, respectively. We run the experiments with at least three independent replicates for each condition.

2.9. Cytoplasmic and nuclear protein extraction

We used the NE-PER Nuclear and Cytoplasmic Extraction Reagents (Thermo Fisher Scientific, 78833) to obtain nuclear and cytoplasmic protein fractions from imatinib-treated HepG2 cells seeded in a 6-well plate (500'000 cells/well). The buffer volumes were chosen according to the pellet size as recommended by the manufacturer's protocol. We first harvested the cells covered with ice-cold cytoplasmic extraction reagent I with a cell scraper, transferred them to a 2 mL-Eppendorf tube, and vortexed each lysate for 15 s. After incubation on ice for 10 min, we added ice-cold cytoplasmic extraction reagent II, vortexed for 5 s, and incubated for 1 min on ice. We subsequently centrifuged the sample (5 min, 16'000 *g*) and obtained the cytoplasmic protein fraction (supernatant). The remaining pellet was further incubated for 40 min on ice in ice-cold nuclear extraction reagent (vortexing every 10 min). After centrifugation (16'000 *g*, 10 min), we obtained the nuclear protein fraction (supernatant). We run the experiment with three independent replicates for each condition and stored the fractions at -80 °C until analysis.

2.10. Quantitative PCR

We run a quantitative PCR to assess the mRNA expression of TFEB-regulated genes in HepG2 cells treated with imatinib for 6 h or 24 h. In brief, we first extracted and purified RNA from imatinib-treated HepG2 cells seeded in a 6-well plate (2×10^6 cells/well) using QIAshredders (Qiagen, 79656) and the Rneasy mini kit (Qiagen, 74104). We determined the purity and concentration of each RNA extract using the NanoDrop One (Thermo Fisher Scientific, Basel, Switzerland) and synthetized complementary DNA of 1 µg RNA with the Omniscript system (Qiagen, 205113). Specific DNA templates were amplified using specific

forward and reverse primers (listed in Table S2) and detected using a DNA double-strand-binding fluorescent dye (FastStart Universal SYBR Green Master, Sigma-Aldrich, 4913914001). We run the qPCR on an ABI PRISM 7700 sequence detector (PE Biosystems, Switzerland) equipped with the ViiA7 software (Life Technologies, Switzerland). We run the experiment with four independent replicates and applied the comparative Ct method (ΔΔCt) to determine the relative mRNA expression normalized to *GAPDH*.

2.11. mTOR/FKBP12 kinase activity in a cell-free assay

The mTOR/FKBP12 Human PIKK Kinase Enzymatic Radiometric Assay (14-769FKKP10) was performed by Eurofins Cerep SA according to their online protocol. In brief, human mTOR/FKBP12 was incubated with 50 mM HEPES (pH 7.5), 1 mM EGTA, 0.01% Tween 20, 2 mg/mL mTOR substrate (C-terminal fragment of p70S6K), 10 μM FKBP12, 3 mM $MnCl_2$, and 10 μM [gamma-33P]-ATP. PI-103, an ATP-competitive mTOR inhibitor, was used as control inhibitor and added to the blank. The reaction was initiated by adding the Mn/ATP mix. After incubation (40 min, room temperature), the reaction was stopped with phosphoric acid to a concentration of 0.5%. Then, 10 μL of the reaction mixture was spotted onto a P30 filter mat and washed four times for 4 min with 0.425% phosphoric acid as well as once with methanol. The sample was dried and subjected to scintillation counting. Eight concentrations in the range of 0.5–100 μM imatinib were tested in triplicates. The counts of the blank containing PI-103 were set as zero, representing full mTOR inhibition. After subtracting the blank, the counts were related to the control, which was considered as 100% active.

2.12. Transmission electron microscopy

We fixed 5 Mio imatinib-treated HepG2 cells (confluency less than 70%) with 1:1 (v/v) cell culture medium/2x fixative mixture (4% paraformaldehyde, 5% glutaraldehyde, in 0.1 M PIPES buffer, pH 7.0, 37 °C) at room temperature. After 20 min, we replaced the medium/2x fixative mixture with fresh 1x fixative mixture (2% paraformaldehyde, 2.5% glutaraldehyde, in 0.1 M PIPES buffer, pH 7.0) and harvested the cells with a cell scraper. The cells were subsequently pelleted (500 *g*, 5 min) and fixed again in fresh 1x fixative mixture (15 min, room temperature). We carefully dislodged the pellet from the tube and continued the fixation (45 min, 4 °C). Then, the cells were pelleted (500 *g*, 5 min), washed three times with 0.1 M PIPES buffer (pH 7.0), and embedded in low-melting point agarose (Sigma-Aldrich, A2576). From the cell-containing solid agarose plug, 1- to 2-mm cubes were trimmed, washed with PBS (10 min), and post-fixed in 1% buffered osmium tetroxide (1h, 4 °C). After rinsing with distilled water, the cubes were stained in aqueous uranyl acetate (1h, 4 °C, protected from light) and subsequently dehydrated in an ethanol (v/v) series (30, 50, 75, 95, and 100%). After three changes of absolute ethanol, the cubes were washed in acetone and embedded in a mixture of resin/acetone followed by pure Epon 812 resin (48 h, 60 °C). Semi-thin sections were cut from the hardened epoxy resin block using a glass knife followed by thinning with a diamond knife. Finally, the thin sections were placed on copper grids, impregnated with uranyl acetate and lead citrate, and analyzed using a FEI Tecnai T12 Transmission Electron Microscope (FEI Technologies Inc., OR, USA) operating at 80 kV. Images were recorded using a CCD Veleta digital camera.

2.13. Annexin V/propidium iodide staining

We used the annexin V Alexa Fluor 488 and propidium iodide (PI) kit (V13245) from Thermo Fisher Scientific to assess the number of apoptotic, necrotic, and viable HepG2 cells after exposure to imatinib. We treated HepG2 cells seeded in a 24-well plate (200'000 cells/well) with imatinib for 6 h and 24 h. Staurosporine (200 nM) and doxorubicin (0.5 μM) were used as positive controls for apoptosis and necrosis, respectively. After the treatment, we harvested the cells with TrypLE express enzyme, transferred them to a V-well plate, and centrifuged the cells (400 *g*, 5 min). The cell pellet was resuspended in 1X annexin-binding buffer (50 μL/well) containing Alexa Fluor 488 annexin V (5 μL/100 μL) as well as PI (0.1 μg/100 μL) and subsequently incubated for 30 min (4 °C, protected from light). HepG2 cells were analyzed with a CytoFLEX flow cytometer. For the flow cytometry gating strategy, singlets were first identified by an FSC-A and an FSC-H gate, and then 10'000 cells per sample were counted in an FSC-A and an SSC-A gate. Apoptotic cells showed green fluorescence (measured in FL-1-A:FITC channel), necrotic cells showed both green and red fluorescence (measured in FL-1-A:FITC and FL-3-A:PC5.5, respectively), while viable cells were not fluorescent. Results were analyzed using the FlowJo software. We run the experiment with four independent replicates.

2.14. Statistical analysis

Experimental data are presented as the mean ± SEM. The number of independent replicates for each experiment is indicated in the respective material and method section. We performed an ANOVA with Dunnett's multiple comparison test using GraphPad prism version 8.2.1 (GraphPad Software, San Diego, USA). Significant values (p-value <0.05) compared to the negative control were indicated with an asterisk (*).

3. Results

3.1. Imatinib and lapatinib increase the volume of the lysosomal compartment

As shown in Fig. 1A, imatinib increased the lysosomal volume in a concentration- and time-dependent manner showing the most pronounced effect at 6 h. After treatment for 0.5 and 6 h, imatinib started to increase the lysosomal volume at 5 μM, reaching significance at ≥10 μM. After treatment for 24 h, imatinib enlarged the lysosomal volume at ≥20 μM. Lapatinib significantly increased the lysosomal volume at concentrations ≥2 μM after ≥0.5 h-treatment with most pronounced effects after 6 h (Fig. 1B). In contrast to imatinib, the increase induced by lapatinib showed a plateau-like effect with increasing concentrations.

Fluorescence microscopy of HepG2 cells (Fig. 1C) and HuH-7 cells (Fig. S1) exposed for 24 h to 10 μM imatinib or 5 μM lapatinib showed that both TKIs strongly increased number and size of lysosomes compared to untreated control cells in both cell lines derived from human hepatomas.

3.2. Imatinib and lapatinib increase the lysosomal pH and perturb the lysosomal proteolytic activity

Next, we assessed the effect of imatinib and lapatinib on the lysosomal pH and membrane integrity by acridine orange (AO) staining. Imatinib redistributed AO into the cytosol at concentrations ≥20 μM after 6 h of treatment, leading to a significantly increased green-to-red AO ratio (Fig. 2A), while concentrations ≤10 μM had no effect on lysosomal pH at both 6 and 24 h. Like imatinib, lapatinib significantly elevated the green-to-red AO ratio at 10 and 20 μM at 6 h, while concentrations ≤5 μM had no effect (Fig. S2A). Thus, both imatinib and lapatinib perturbed the lysosomal pH and/or membrane stability in a concentration-dependent manner, with significant changes at the two highest concentrations tested.

Lysosomes contain more than 60 hydrolases (e.g., proteases), whose optimal activities are in an acidic environment (Xu and Ren, 2015). Since an increased lysosomal pH could impair protease activity, we investigated the effect of the TKIs on lysosomal protein degradation using fluorescent DQ-BSA. Bafilomycin A1, chloroquine, and amiodarone increased the percentage of cells with low (DQ-BSA^{neg} cells) lysosomal proteolytic activity, while the mTORC1 inhibitor rapamycin increased the percentage of cells with high (DQ-BSA^{high} cells) lysosomal

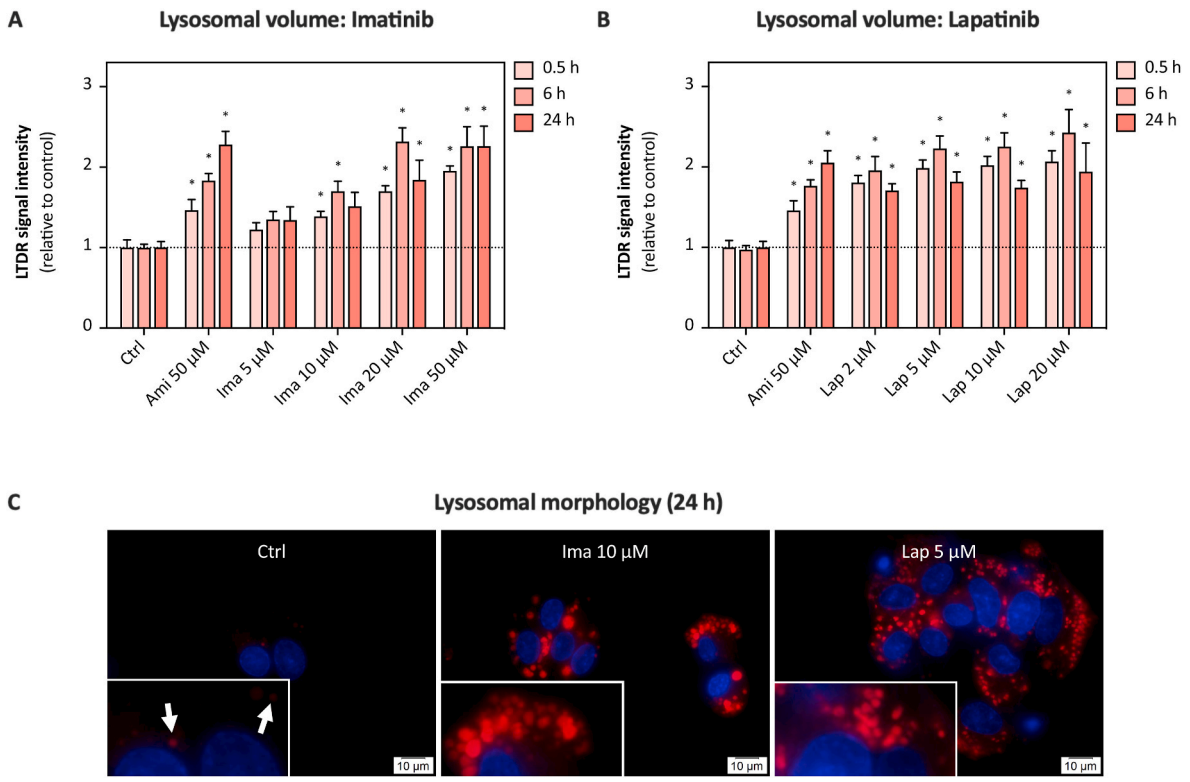

Fig. 1. Lysosomal volume and morphology. The volume of the lysosomal compartment was assessed by LysoTracker Deep Red (LTDR) staining in HepG2 cells treated with (**A**) imatinib (5–50 µM) and (**B**) lapatinib (2–20 µM) for 0.5 h, 6 h, and 24 h. Data are shown as fold increase relative to the negative control (ctrl) and are the mean ± SEM of at least five independent replicates. *p < 0.05 versus negative control. (**C**) Representative microscopic pictures of untreated HepG2 cells (ctrl) and HepG2 cells treated with 10 µM imatinib or 5 µM lapatinib for 24 h. Lysosomes (red) and nuclei (blue) were stained with LTDR and Hoechst 33342, respectively. Ima: Imatinib; Lap: lapatinib; Ami: amiodarone (positive control).

proteolytic activity (Figs. S3A and S3B). Imatinib significantly increased the percentage of DQ-BSA^{high} cells up to 20 µM at both 6 and 24 h, while 50 µM imatinib abolished the lysosomal proteolytic activity at both time points (Figs. S3A and S3B). Similarly, HepG2 cells exposed to lapatinib for 6 and 24 h showed a significantly increased lysosomal proteolytic activity up to 20 µM (Figs. S3A and S3B), while 24 h-treatment with 20 µM lapatinib resulted in a significant population of DQ-BSA^{neg} cells.

Since both imatinib and lapatinib increased the volume of the lysosomal compartment, we normalized the DQ-BSA signal intensity to the lysosomal volume. Upon normalization, 5 µM imatinib had no significant effect on lysosomal proteolytic activity, whereas 10 µM imatinib enhanced lysosomal proteolysis up to 6 h, but not up to 24 h (Fig. 2B). In comparison, 20 µM imatinib started to decrease lysosomal proteolytic activity at 24 h, and 50 µM imatinib after ≥6 h. For lapatinib, we observed a decreased lysosomal proteolytic activity starting at 20 µM (Fig. S2B). The decreased lysosomal protease activity at ≥20 µM imatinib and lapatinib corresponds to the observed increase in lysosomal pH at these concentrations. Since the effects of lapatinib on lysosomal morphology and function were less pronounced compared to imatinib, the following investigations were performed only for imatinib.

3.3. Imatinib interferes with cathepsin B activation

CTSB, one of the main lysosomal cysteine proteases, is synthetized as an inactive pro-enzyme in the endoplasmic reticulum and, while being transported to the lysosomes, processed to an active single chain form (Kominami et al., 1988). In the lysosome, the single chain (sc) is further processed to a two-chain form composed of a heavy (hc) and light chain. As shown in Fig. 2C and D, the expression of the sc-CTSB increased in a concentration-dependent manner up to 20 µM imatinib but dropped at 50 µM. In comparison, the expression of the hc-CTSB was significantly decreased at imatinib concentrations ≥5 µM. Total (sc- & hc-CTSB) CTSB was not affected up to 20 µM imatinib, while 50 µM caused a significant drop (Fig. S2C).

Accumulation of sc-CTSB and decreased formation of hc-CTSB indicated impairment of lysosomal proteolytic processing of CTSB by imatinib, confirming the results of the previous section.

3.4. Imatinib induces nuclear translocation of TFEB and upregulates the expression of lysosomal genes

Lysosomal dysfunction can activate the transcription factor TFEB, which stimulates lysosomal biogenesis (Puertollano et al., 2018). Under normal conditions, TFEB is phosphorylated and retained in the cytoplasm, while stressors such as starvation reduce phosphorylation and favor translocation into the nucleus (Puertollano et al., 2018). As shown in Fig. 3A and B, imatinib caused a decrease in cytoplasmic TFEB starting at 6 h and 5 µM, reaching statistical significance at ≥20 µM. In parallel, TFEB gradually accumulated in the nuclear fraction, reaching significance at ≥20 µM imatinib. In comparison, treatment for 0.5 h stimulated the import of TFEB into the nucleus only at the highest imatinib concentration (Fig. S4).

Nuclear TFEB binds to specific palindromic 10-base pair DNA sequences called coordinated lysosomal expression and regulation (i.e., CLEAR) elements (Sardiello et al., 2009), which are present in promotors of various genes encoding lysosomal proteins. Thus, we quantified the mRNA expression of the lysosomal associated membrane protein 1 (*LAMP1*), the ATPase H^+ transporting V1 subunit H (*ATP6V1H*), and

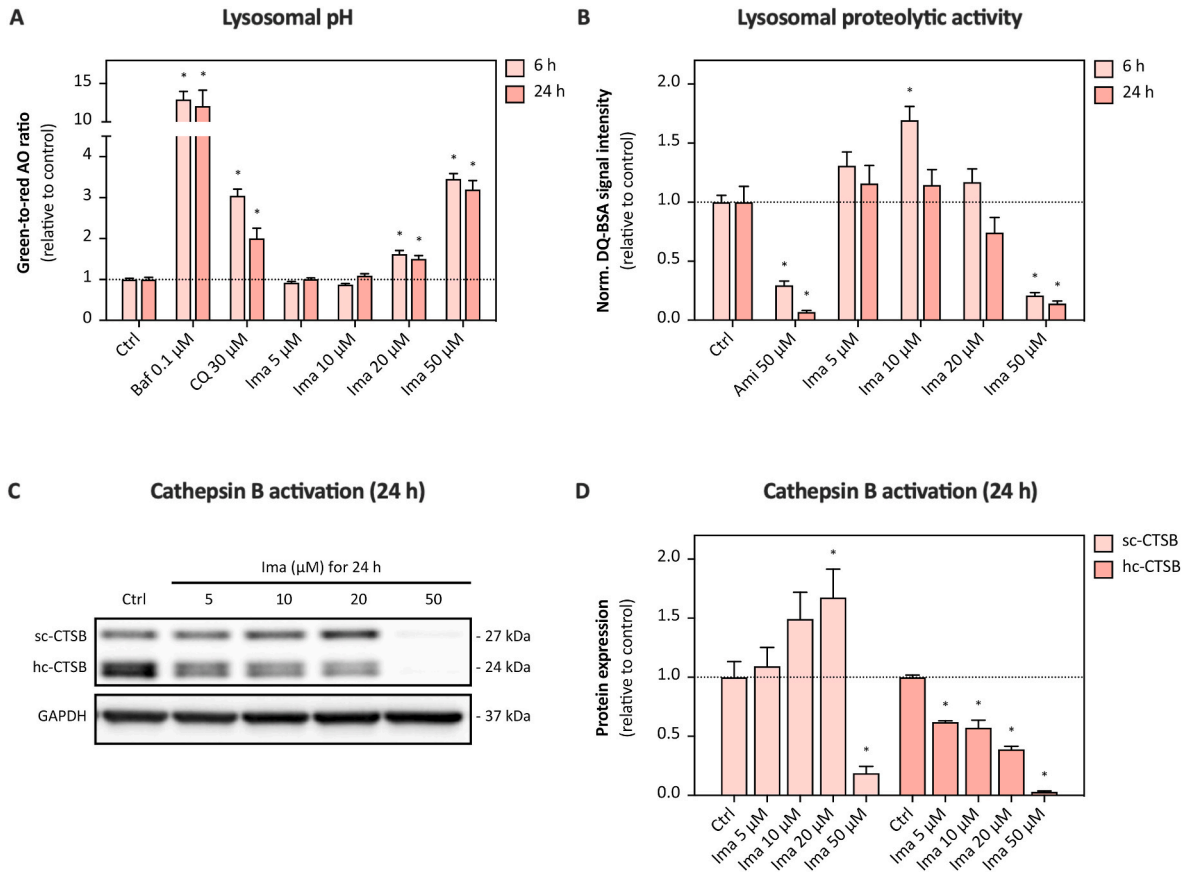

Fig. 2. Lysosomal pH and proteolytic activity. (**A**) Lysosomal pH assessed by acridine orange (AO) staining (ratio of green-to-red fluorescence) in HepG2 cells treated with imatinib (5–50 µM) for 6 h and 24 h. Bafilomycin A1 (Baf) and chloroquine (CQ) represent the positive controls. Data are shown as fold increase relative to the negative control (ctrl) and are the mean ± SEM of at least three independent replicates. *p < 0.05 versus negative control. (**B**) Lysosomal proteolytic activity assessed by DQ-BSA staining (normalized to the lysosomal volume) in HepG2 cells treated with imatinib (5–50 µM) for 6 h and 24 h. Amiodarone (Ami) represents the positive control. Data are shown as fold increase relative to the negative control (ctrl) and are the mean ± SEM of five independent replicates. *p < 0.05 versus negative control. (**C**) Representative Western blot and (**D**) quantification of cathepsin B (CTSB) in HepG2 cells treated with imatinib (5–50 µM) for 24 h. Single-chain (sc) CTSB and heavy-chain (hc) CTSB represent differently processed CTSB forms. GAPDH represents the loading control. Data are shown as fold increase relative to the negative control (ctrl) and are the mean ± SEM of four independent replicates. *p < 0.05 versus negative control. Ima: Imatinib.

cathepsin B (*CTSB*) in HepG2 cells exposed to imatinib for 6 h (Figs. 3C) and 24 h (Fig. 3D). Treatment with imatinib for 6 h did not affect mRNA expression of *LAMP1*, *ATP6V1H*, and *CTSB* (Fig. 3C), whereas their mRNA expression was increased at imatinib concentrations ≥10 µM after 24 h (Fig. 3D).

3.5. Imatinib reduces the activity of mTORC1

To investigate closer the mechanism of TFEB activation, we assessed the activity of the protein complex mTORC1 in imatinib-treated HepG2 cells. Among other kinases (i.e., AKT serine/threonine kinase 1 [AKT1], glycogen synthase kinase 3 beta [GSK3B], mitogen-activated protein kinase 1/3 [MAPK1/3]), mTORC1 is considered as the main negative regulator of TFEB activity (Roczniak-Ferguson et al., 2012). We evaluated the activity of mTORC1 in imatinib-treated HepG2 cells by assessing the phosphorylation state of Unc-51 like autophagy activating kinase 1 (ULK1), ribosomal protein S6 (RPS6), and eukaryotic translation initiation factor 4E binding protein 1 (EIF4EBP1), three well-established mTORC1 substrates (Kim et al., 2011; Sanvee et al., 2019). Upon treatment for 6 h, the phosphorylation of ULK1 (S757), RPS6 (S235/236), and EIF4EBP1 (S65) decreased in a concentration-dependent manner starting at 10 µM imatinib and reaching significance at ≥20 µM (Fig. 4A and B). The activity of mTORC1 further decreased with treatment for 24 h (Fig. 4C and D). After 0.5 h, the activity of mTORC1 was reduced at 50 µM imatinib (Fig. S5).

3.6. Imatinib does not impair the activity of activating kinases upstream of mTORC1

mTORC1 is activated on the lysosomal membrane by the GTPase RHEB, the activity of which is inhibited by the TSC complex (TSC1/2) (Sancak et al., 2010). Since TSC1/2 activity is regulated by AKT1, MAPK1/3, and PRKAA, a reduced activity of one of these kinases could impair mTORC1 activity (Kwiatkowski and Manning, 2005). AKT1 is activated by phosphorylation at T308 and S473 by the insulin signaling pathway and mTORC2, respectively (Sanvee et al., 2019). Imatinib treatment for 24 h increased the phosphorylation of AKT1 in a concentration-dependent manner starting at 5 µM for S473 and at 10 µM for T308 (Fig. 5A and B), while treatment for 6 h numerically enhanced the serine site phosphorylation at ≥20 µM (Figs. S6A and S6B). Beside TSC1/2, AKT1 phosphorylates GSK3B at S9, leading to GSK3B inactivation. Imatinib increased the phosphorylation of GSK3B (S9) in a concentration-dependent manner, reaching significance at ≥20 µM (Fig. 5A and B). Similar to AKT1, the phosphorylation of MAPK1/3 at T202 and Y204 increased, reaching the highest effects at 50 µM and 20 µM imatinib after 6 h (Fig. S6A and S6C) and 24 h (Fig. 5C and D), respectively. PRKAA, which is activated by phosphorylation at T172, showed no increase in T172 phosphorylation at both treatment times (Fig. 5C and D, Figs. S6A and S6C). While AKT1 and MAPK1/3 inhibit

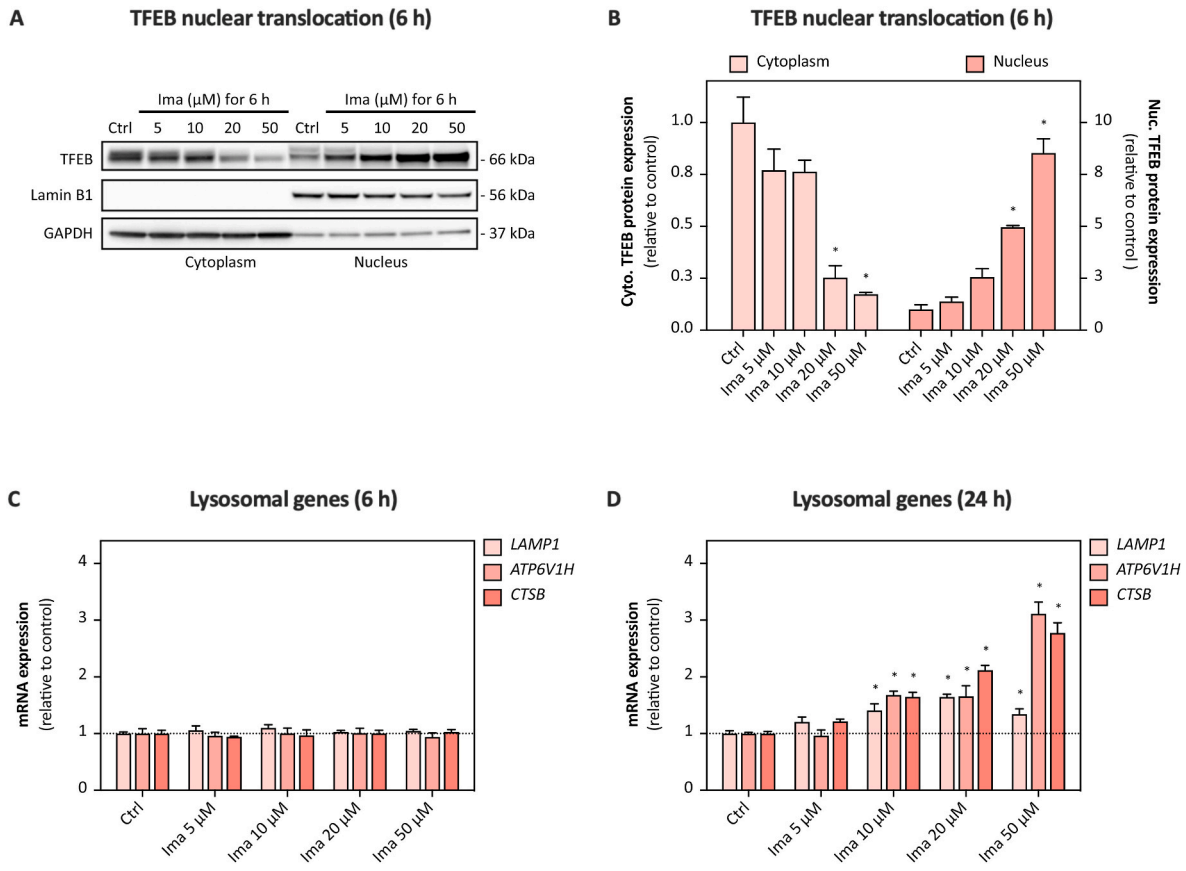

Fig. 3. Activation of transcription factor EB (TFEB). (**A**) Representative Western blot and (**B**) quantification of TFEB in cytoplasmic and nuclear fraction of HepG2 cells treated with imatinib (5–50 μM) for 6 h. Lamin B1 and GAPDH served as nuclear and cytoplasmic loading control, respectively. Data are shown as fold increase relative to the negative control (ctrl) and are the mean ± SEM of three independent replicates. *$p < 0.05$ versus negative control. Gene expression of lysosomal genes (*LAMP1*, *ATP6V1H*, *CTSB*) in HepG2 cells treated with imatinib (5–50 μM) for (**C**) 6 h and (**D**) 24 h. Data are shown as fold increase relative to the negative control (ctrl) and are the mean ± SEM of four independent replicates. *$p < 0.05$ versus negative control. Ima: Imatinib; *LAMP1*: Lysosomal associated membrane protein 1; *ATP6V1H*: ATPase H^+ transporting V1 subunit H; *CTSB*: Cathepsin B.

the activity of TSC1/2, PRKAA acts as an activator. Thus, inhibition of mTORC1 by imatinib did not result from AKT1 or MAPK1/3 inactivation or PRKAA activation. Moreover, a cell-free assay of the mTORC1 activity excluded a direct inhibition of mTORC1 by imatinib (Fig. 5E). This means that lysosomal dysfunction is the most probable explanation for impaired function of mTORC1 in HepG2 cells treated with imatinib.

3.7. Imatinib induces the transcription of autophagy genes and initiates autophagy

mTORC1 and TFEB connect lysosomal biogenesis to autophagy, a catabolic process by which unnecessary or dysfunctional cytoplasmic components are delivered to lysosomes for degradation (Settembre et al., 2011). To study the effect of imatinib on autophagy, we assessed the mRNA expression of beclin 1 (*BECN1*), sequestosome 1 (*SQSTM1*), microtubule associated protein 1 light chain 3 beta (*MAP1LC3B*), and UV radiation resistance associated gene (*UVRAG*), whose expression is controlled by TFEB. Upon treatment for 6 h, imatinib increased the expression of these genes at concentrations ≥20 μM (Fig. 6A), which is in line with TFEB nuclear translocation described above. After 24 h, the expression of *BECN1*, *SQSTM1*, *MAP1LC3B*, and *UVRAG* further increased, reaching significance ≥10 μM imatinib (Fig. 6B).

In mammalian cells, autophagy is initiated by a protein complex composed of ULK1, autophagy related protein 13 (ATG13), ATG101, and the focal adhesion kinase interacting protein of 200 kDa. Impaired activity of mTORC1 stimulates ULK1, which activates ATG13 by phosphorylation at S318 (Egan et al., 2015). Imatinib increased the phosphorylation of ATG13 (S318) starting at 5 μM, reaching significance at 10 and 20 μM upon 6 h of treatment (Fig. 7A and B). At 24 h, phosphorylation of ATG13 S318 was significantly increased at 5–20 μM imatinib and more pronounced than after 6 h (Fig. 7C and D).

Initiation of autophagy leads to the formation of new autophagosomes. The lipidated form of MAP1LC3A/B is integrated in the autophagosomal membranes and can be used as a marker for autophagosome accumulation (Klionsky et al., 2016). The 6 h-treatment with imatinib increased MAP1LC3A/B-II expression at 5 and 10 μM imatinib (Fig. 7A and B). After 24 h, the expression of MAP1LC3A/B-II was significantly increased at concentration between 5 and 20 μM imatinib and more pronounced than after 6 h (Fig. 7C and D), indicating accumulation of autophagosomes over time. The expression of the autophagy adaptor protein SQSTM1 significantly increased after 24 h imatinib exposure at ≥5 μM (Fig. 7C and D), while no increase was observable after 6 h (Fig. 7A and B).

To qualitatively assess the accumulation of autophagic vacuoles (e.g., autophagosomes, autolysosomes), we acquired electron micrographs of imatinib-treated HepG2 cells. A concentration of 10 μM imatinib applied for 24 h increased the number of autophagosomes (i.e., membrane-bound vacuoles containing morphologically intact cytoplasmic material) in HepG2 cells compared to the control cells (Fig. 7E). Among other materials, the autophagosomes of HepG2 cells treated with 10 μM imatinib contained electron-dense lysosomes. Chloroquine (30 μM) increased the size of lysosomes and prevented the degradation of autophagic cargo, which can be explained by the reduced lysosomal proteolytic activity (Fig. S3B). In contrast to control cells and HepG2

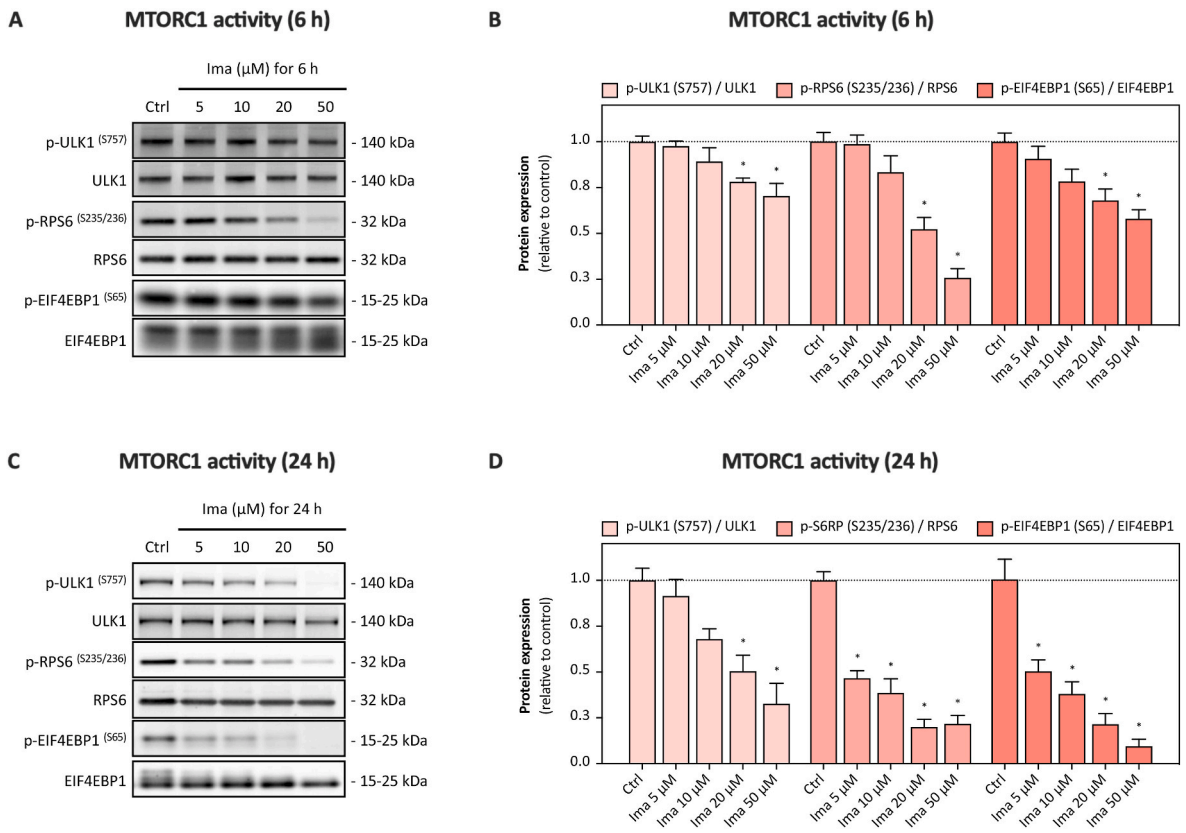

Fig. 4. Activity of mTOR complex 1 (mTORC1). (**A**, **C**) Representative Western blots and (**B**, **D**) quantification of phosphorylated mTORC1 substrates (ULK1, RPS6, and EIF4EBP1) in HepG2 cells treated with imatinib (5–50 μM) for (**A**, **B**) 6 h and (**C**, **D**) 24 h. The phosphorylation states of ULK1 (S7575), RPS6 (S235/236), and EIF4EBP1 (S65) were assessed using phospho-specific antibodies and normalized to the expressions of the total protein. Data are shown as fold increase relative to the negative control (ctrl) and are the mean ± SEM of at least three independent replicates. *p < 0.05 versus negative control. Ima: Imatinib; ULK1: Unc-51 like autophagy activating kinase 1; RPS6: Ribosomal protein S6; EIF4EBP1: Eukaryotic translation initiation factor 4E binding protein 1.

cells treated with chloroquine, imatinib-treated cells comprised also electron-translucent vacuoles containing cytoplasmic material at various stages of degradation, representing active autolysosomes.

3.8. Imatinib induces apoptosis in HepG2 cells in a concentration-dependent manner

Release of lysosomal hydrolases into the cytoplasm upon permeabilization of the lysosomal membrane and accumulation of undegraded material can induce apoptosis and necrosis (Boya and Kroemer, 2008). Having observed a disturbed lysosomal function, we finally assessed the effect of imatinib on cell death in HepG2 cells using the annexin V/PI staining. As expected, imatinib induced apoptosis in a concentration-dependent manner with a significant number of apoptotic cells at 50 μM after both 6 h and 24 h (Fig. 8A). Induction of apoptosis was by trend more pronounced at 6 than at 24 h, while necrosis was more pronounced after 24 h (Fig. 8B). Overall, the number of viable cells significantly decreased at imatinib concentrations ≥20 μM (Fig. 8C).

4. Discussion

The present study shows that the TKIs imatinib and lapatinib disturb lysosomal function and morphology in human hepatoma-derived cell lines, as demonstrated by an increase in the lysosomal volume fraction, perturbed lysosomal pH, and impaired proteolytic activity. Imatinib-induced lysosomal dysfunction was accompanied by activation of TFEB and impaired mTORC1 activity, which stimulated autophagy and apoptosis.

Imatinib is typically administered at doses of 400–800 mg daily, leading to steady state plasma concentrations in the range of 3.6–6.9 μM (Peng et al., 2005). Since imatinib is metabolized via cytochrome P450 3A4/5, inhibitors of these enzymes increase the plasma and probably also the hepatic concentrations of imatinib (Peng et al., 2005). For lapatinib, maximal plasma concentrations are between 4.1 and 7.4 μM and could also be higher when combined with cytochrome P450 3A4 inhibitors (Chu et al., 2007). In mice, the hepatic concentrations of imatinib and lapatinib have been reported to exceed the corresponding plasma concentrations by a factor of 5–10 (Gardner et al., 2009; Hudachek and Gustafson, 2013). Based on these considerations, most effects observed in the current investigations could therefore be relevant for patients treated with these drugs.

Lysosomotropic drugs are structurally diverse molecules of different drug classes including TKIs, which accumulate in acidic organelles (Nadanaciva et al., 2011). Lysosomes attract lipophilic, weakly basic drugs, which passively cross cell membranes in their neutral form and become trapped upon protonation, a phenomenon described as lysosomotropism (de Duve et al., 1974). Both imatinib and lapatinib are known to accumulate in lysosomes of several human cancer cell lines (Burger et al., 2015; Fu et al., 2014). For instance, in CML cells incubated for 1 h with 20 μM imatinib, the drug achieved lysosomal concentrations in the millimolar range (Fu et al., 2014). Similarly, Burger and co-workers found in several cell lines that after 0.5 h of incubation with imatinib the intracellular imatinib concentrations were 35- to >100-fold higher than in the incubation medium (Burger et al., 2015). The lysosomal accumulation occurred rapidly within 15 min and could be prevented by bafilomycin A1 (Burger et al., 2015), a proton pump V-ATPase

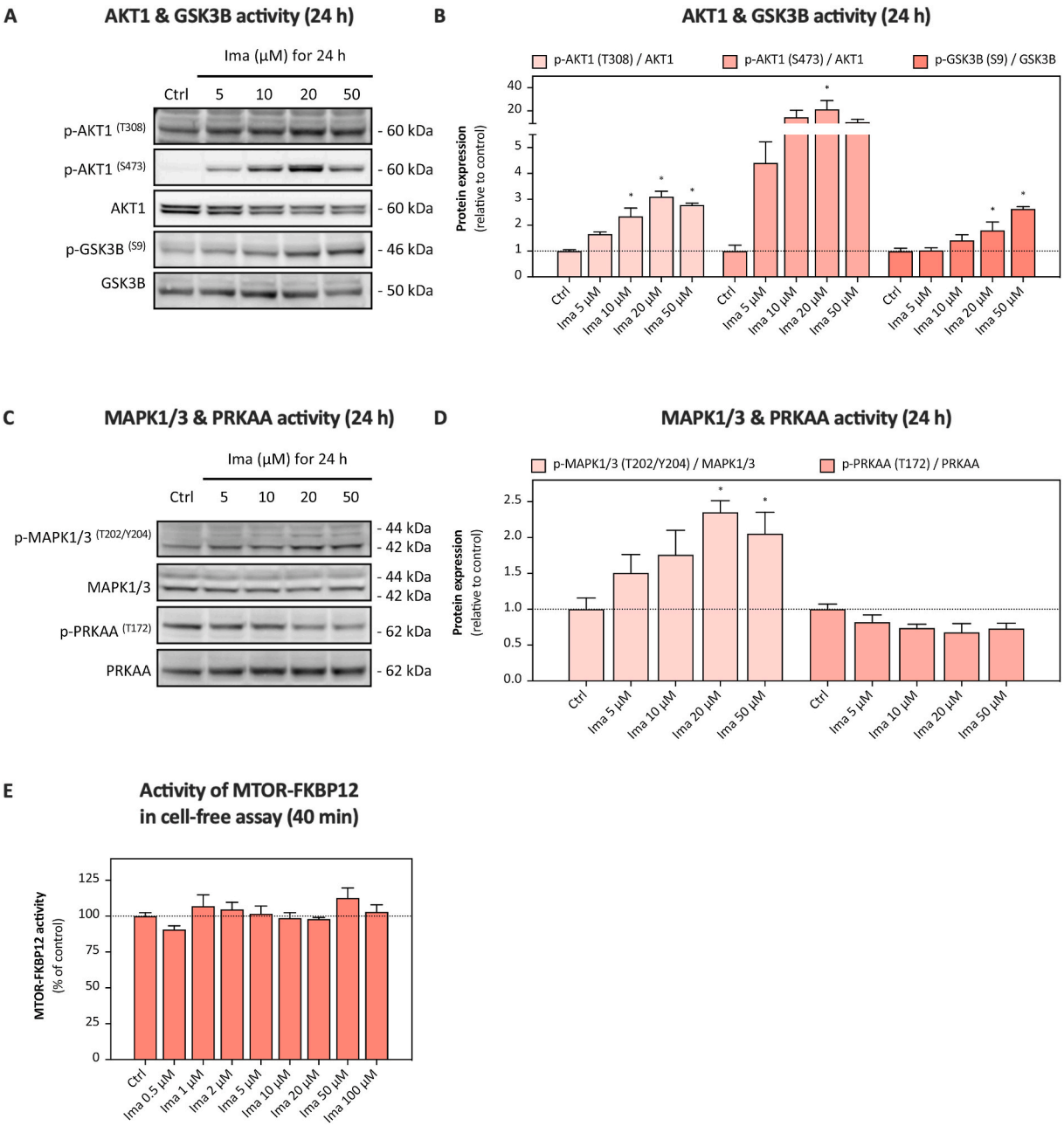

Fig. 5. Activity of kinases upstream of mTORC1 and mTORC1 activity in a cell-free assay. (**A**) Representative Western blots and (**B**) quantification of corresponding phosphorylation states of AKT1 and GSK3B in HepG2 cells treated with imatinib (1–50 μM) for 24 h. The phosphorylation of AKT1 (T308), AKT1 (S473), and GSK3B (S9) were assessed using phospho-specific antibodies and normalized to the expressions of the total protein. Data are shown as fold increase relative to the negative control (ctrl) and are the mean ± SEM of three to four independent replicates. *p < 0.05 versus negative control. (**C**) Representative Western blots and (**D**) quantification of corresponding phosphorylation states of MAPK1/3 and PRKAA1 in HepG2 cells exposed to imatinib (5–50 μM) for 24 h. The phosphorylation of MAPK1/3 (T202/Y204) and PRKAA (T172) were assessed using phospho-specific antibodies and normalized to the expressions of the total protein. Data are shown as fold increase relative to the negative control (ctrl) and are the mean ± SEM of three to four independent replicates. *p < 0.05 versus negative control. (**E**) Activity of mTOR-FKBP12 (assessed by the phosphorylation of the mTORC1 substrate p70S6K) in a cell-free, enzymatic assay upon incubation with imatinib for 40 min. Data are shown as percentage (%) of the negative control (ctrl) and are the mean ± SEM of three replicates. Ima: Imatinib; AKT1: AKT serine/threonine kinase 1; GSK3B: Glycogen synthase kinase 3 beta; MAPK1/3: Mitogen-activated protein kinase 1/3; PRKAA: Protein kinase AMP-activated catalytic subunit alpha 1 and 2; FKBP12: 12.6 kDa FK506-binding protein; p70S6K: 70 kDa ribosomal protein S6 kinase 1.

inhibitor, or by chloroquine (Fu et al., 2014), a stronger base than imatinib, confirming that the pH gradient is the driving force of this phenomenon.

Accumulation of lysosomotropic drugs in lysosomes is typically accompanied by an enlargement of the organelle (Funk and Krise, 2012; Lu et al., 2017), a cell type-independent effect already described for imatinib (Ertmer et al., 2007). We previously reported an increase in lysosomal volume in HepG2 cells by ponatinib, regorafenib, and sorafenib (Paech et al., 2018). In the present study, imatinib and lapatinib increased the lysosomal volume fraction after 0.5 h of incubation (Fig. 1A and C), a result in line with the reported rapid intracellular accumulation of imatinib (Burger et al., 2015). Fluorescence microscopy revealed that the size of lysosomes in cells exposed to imatinib or lapatinib largely exceeded the typical lysosomal size of 0.5–1 μm (Xu

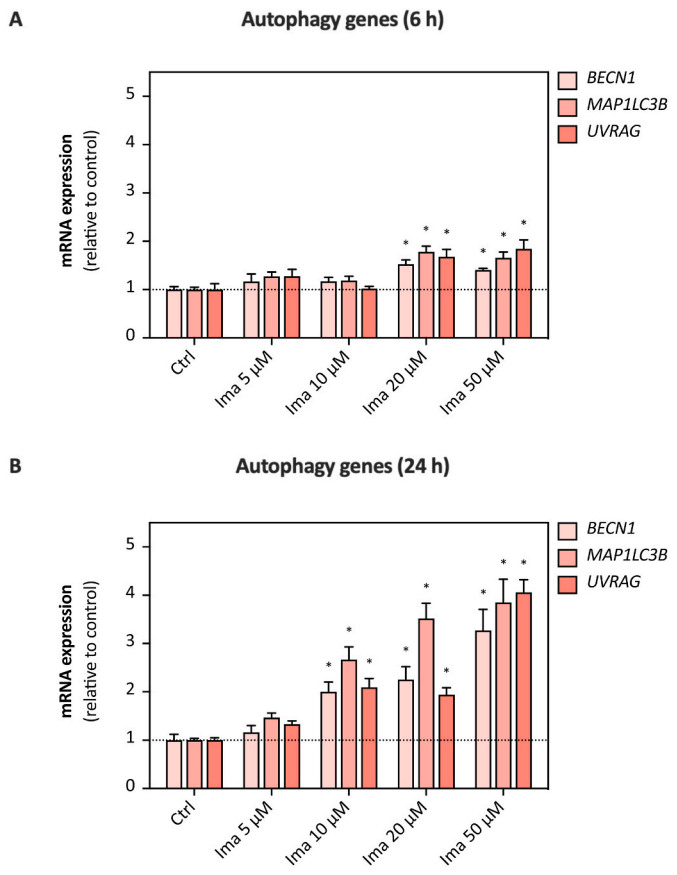

Fig. 6. Expression of autophagy genes. Gene expression of autophagic genes (*BECN1*, *SQSTM1*, *MAP1LC3B*, *UVRAG*) in HepG2 cells treated with imatinib (5–50 µM) for (**A**) 6 h and (**B**) 24 h. Data are shown as fold increase relative to the negative control (ctrl) and are the mean ± SEM of four independent replicates. *p < 0.05 versus negative control. Ima: Imatinib; *BECN1*: Beclin 1; *SQSTM1*: Sequestosome 1; *MAP1LC3B*: Microtubule associated protein 1 light chain 3 beta; *UVRAG*: UV radiation resistance associated gene protein.

and Ren, 2015). Osmotic water influx, impaired lysosomal vesicle trafficking, intercalation into the lysosomal membrane, and stimulated biogenesis are proposed mechanisms explaining an expansion of the lysosomal compartment (Morissette et al., 2008; Sardiello et al., 2009; Skoupa et al., 2020). In the current study, the rapid increase in lysosomal volume after exposure to imatinib or lapatinib is explained best by osmotic swelling, whereas intercalation into the lysosomal membrane and increased biogenesis may have contributed at later time points. As shown in the current and in a previous investigation (Paech et al., 2018), lysosomal accumulation of TKIs depends on the amphiphilic nature of these drugs, but not on the tyrosine kinase inhibited. The toxicity associated with lysosomal accumulation of TKIs may lead to adverse reactions such as hepatotoxicity and/or enhance the therapeutic efficacy of these drugs when tumor cells are affected.

Lysosomal biogenesis is regulated by mTORC1 and TFEB (Sardiello et al., 2009; Settembre et al., 2011). Since neither mTORC1 (Fig. S5) nor TFEB (Fig. S4) were affected after 0.5 h of exposure to imatinib, the early increase in the lysosomal volume cannot be explained by stimulation of biogenesis. However, after 6 h of exposure to imatinib, we observed impaired activity of mTORC1 and nuclear translocation of TFEB as well as increased transcription of lysosomal genes after 24 h, indicating stimulation of lysosomal biogenesis. At 24 h of exposure to imatinib and lapatinib, the lysosomal volume was generally numerically lower than at 6 h, which may be explained by the toxicity of these drugs. Similar to our findings, Skoupa and co-workers found that imatinib treatment for 6 h expanded the lysosomal volume in leukemia cells (Skoupa et al., 2020). However, they found no stimulation of lysosomal biogenesis and proposed Ca^{2+}-dependent lysosomal fusion as the principal mechanism. Furthermore, Lu and co-worker showed that chloroquine increased the protein expression of the lysosomal marker LAMP2 after 24 but not after 4 h, despite nuclear translocation of TFEB already after 1 h (Lu et al., 2017).

We not only observed an increase in lysosomal volume, but also an impairment of lysosomal function as evidenced by an elevation in the lysosomal pH and impaired proteolytic capacity. While the transiently increased degradation of DQ-BSA at low imatinib and lapatinib concentrations could be attributed to the raised lysosomal volume and proteolytic capacity, the decreased proteolytic activity at higher concentrations and longer exposure reflects a loss of lysosomal function. Lysosomes can degrade protein complexes and organelles through the autophagy-lysosome pathway (Klionsky et al., 2016). A dysfunction in this catabolic capacity has been associated with cell and organ damage, which can also affect the liver (Hara et al., 2006). Long-term treatment with imatinib and lapatinib could potentially decrease the hepatic degradation of long-lived proteins, as it has been observed for instance for siramesine (Ostenfeld et al., 2008).

As shown for concanamycin A and bafilomycin A1, a disturbed lysosomal function is associated with impaired activity of mTORC1 (Ostenfeld et al., 2008). When lysosomes function normally, mTOR is recruited to the lysosomal membrane in response to an increase in the amino acid concentration by four RRAG GTPases (RRAG A, B, C, and D) and LAMTOR, which is anchored in the lysosomal membrane through lipidation (Nada et al., 2009). Knock-down of RRAGC caused nuclear localization of TFEB, demonstrating that impaired docking of mTOR on the lysosomal surface is sufficient to stimulate TFEB nuclear translocation (Roczniak-Ferguson et al., 2012). Moreover, RHEB, the activator of mTORC1, is also attached to the lysosomal membrane (Sancak et al., 2010). Thus, damage of the lysosomal membrane, e.g., by fluidization, is a proposed mechanism of lysosomotropic drug-induced mTORC1 inhibition and TFEB activation (Zhitomirsky et al., 2018). Mechanistically, the hydrophobic ring-structure of imatinb could be incorporated into the lysosomal membrane, while the protonated amine group would face the lysosomal lumen. These detergent-like properties of lysosomotropic compounds could impair the integrity of the lysosomal membrane, as it has been shown for siramesine (Ostenfeld et al., 2008). Moreover, sequestration of lysosomes into autophagic vacuoles (Fig. 7E) diminishes the accessibility of this organelle for the recruitment of mTORC1. Since we have excluded impairment of the function of the main kinases responsible for mTORC1 phosphorylation and direct inhibition of mTORC1 by imatinib, disturbed lysosomal function appears to be most probable mechanism impairing the activation of mTORC1 by imatinib.

Beside by mTORC1, TFEB can be phosphorylated (and retained in the cytoplasm) by MAPK1, GSK3B, and AKT1 (Puertollano et al., 2018). The activities of AKT1 and MAPK1 were increased by imatinib (Fig. 5A–D, Fig. S6), excluding them as a cause for impaired TFEB phosphorylation. The phosphorylation of GSK3B was also increased in the presence of imatinib (Fig. 5A and B), inhibiting GSK3B activity. Impaired GSK3B activity could therefore have contributed to the imatinib-induced nuclear translocation of TFEB.

Inhibition of mTORC1, a well-established inhibitor of autophagy, and upregulation of the CLEAR gene network by TFEB are expected to stimulate autophagy in mammalian cells (Kim et al., 2011; Settembre et al., 2011). Accordingly, we observed activation of ULK1 (Fig. 4) and ATG13 (Fig. 7), upregulation of autophagic genes (Fig. 6) and increased levels of MAP1LC3A/B-II (Fig. 7) in HepG2 cells upon imatinib treatment. Our findings are in line with an earlier report that suggested stimulation of autophagy by imatinib in several mammalian cell types (Ertmer et al., 2007). However, the increased lysosomal pH and the impaired proteolysis suggest that the autophagic flux in the presence of imatinib is incomplete at a certain drug concentration. Several lysosomotropic drugs are known to be associated with ineffective autophagy

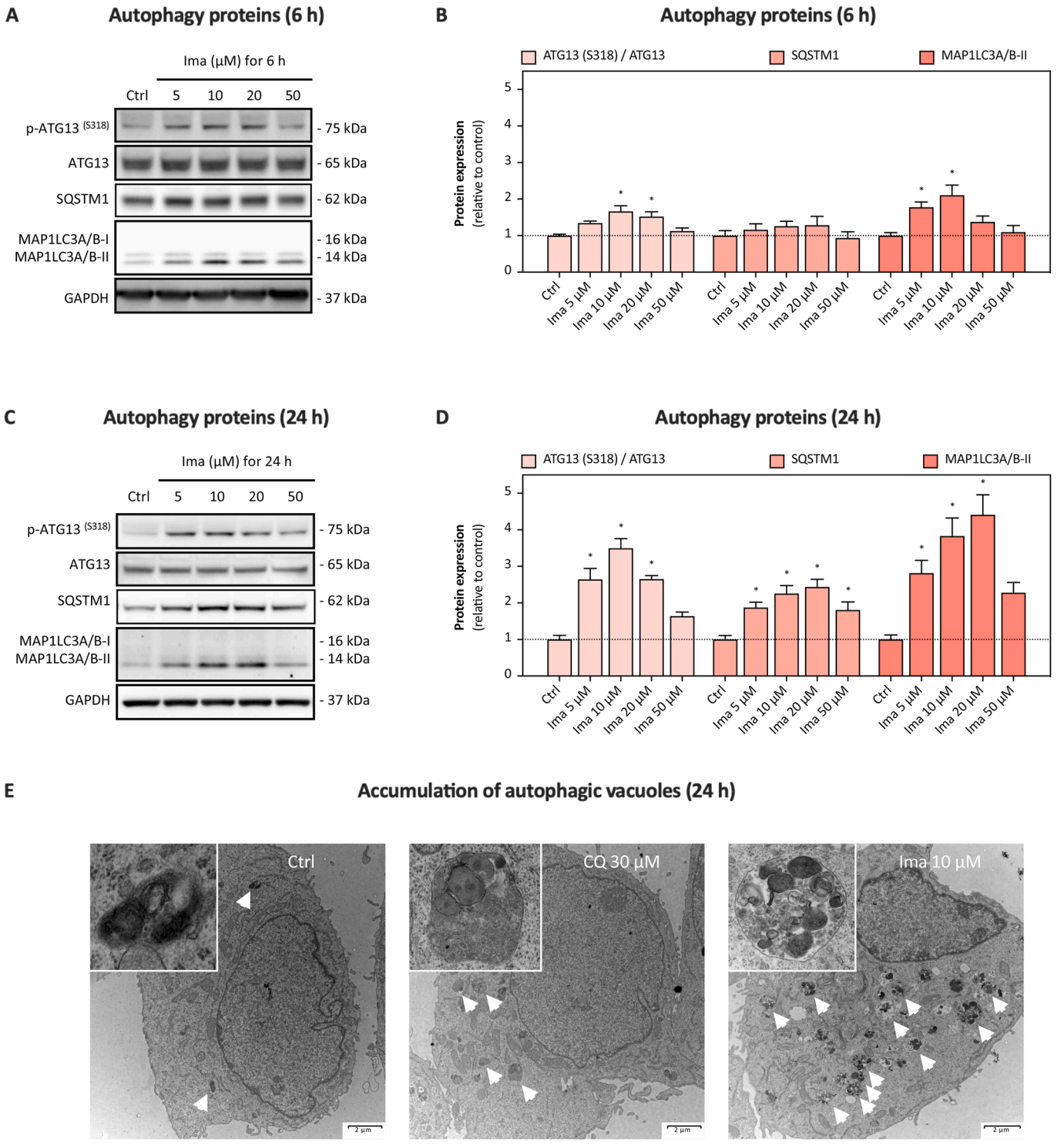

Fig. 7. Expression of autophagy proteins. (**A**) Representative Western blots and (**B**) quantification of phosphorylated ATG13 (S318), SQSTM1 and MAP1LC3A/B-I/II in HepG2 cells treated with imatinib (5–50 μM) for 6 h. The phosphorylation of ATG13 (S318) was assessed using a phospho-specific antibody and normalized to the expression of the total protein. Data are shown as fold increase relative to the negative control (ctrl) and are the mean ± SEM of three to four independent replicates. *$p < 0.05$ versus negative control. (**C**) Representative Western blots and (D) quantification of phosphorylated ATG13 (S318), SQSTM1 and MAP1LC3A/B-I/II in HepG2 cells treated with imatinib (5–50 μM) for 24 h. The phosphorylation of ATG13 (S318) was assessed using a phospho-specific antibody and normalized to the expression of the total protein. Data are shown as fold increase relative to the negative control (ctrl) and are the mean ± SEM of three to four independent replicates. *$p < 0.05$ versus negative control. (**E**) Representative electron microscopy micrographs of control (ctrl) HepG2 cells and cells exposed to chloroquine (30 μM) and imatinib (10 μM) for 24 h. The arrows indicate lysosomes (electron-dense, black vesicles) and autophagic vesicles (e.g., autophagosomes, autolysosomes). The scale bar represents a length of 2 μm. Ima: Imatinib; ATG13: Autophagy related protein 13; SQSTM1: Sequestosome 1; MAP1LC3A/B: Microtubule associated protein 1 light chain 3 alpha/beta, CQ: Chloroquine.

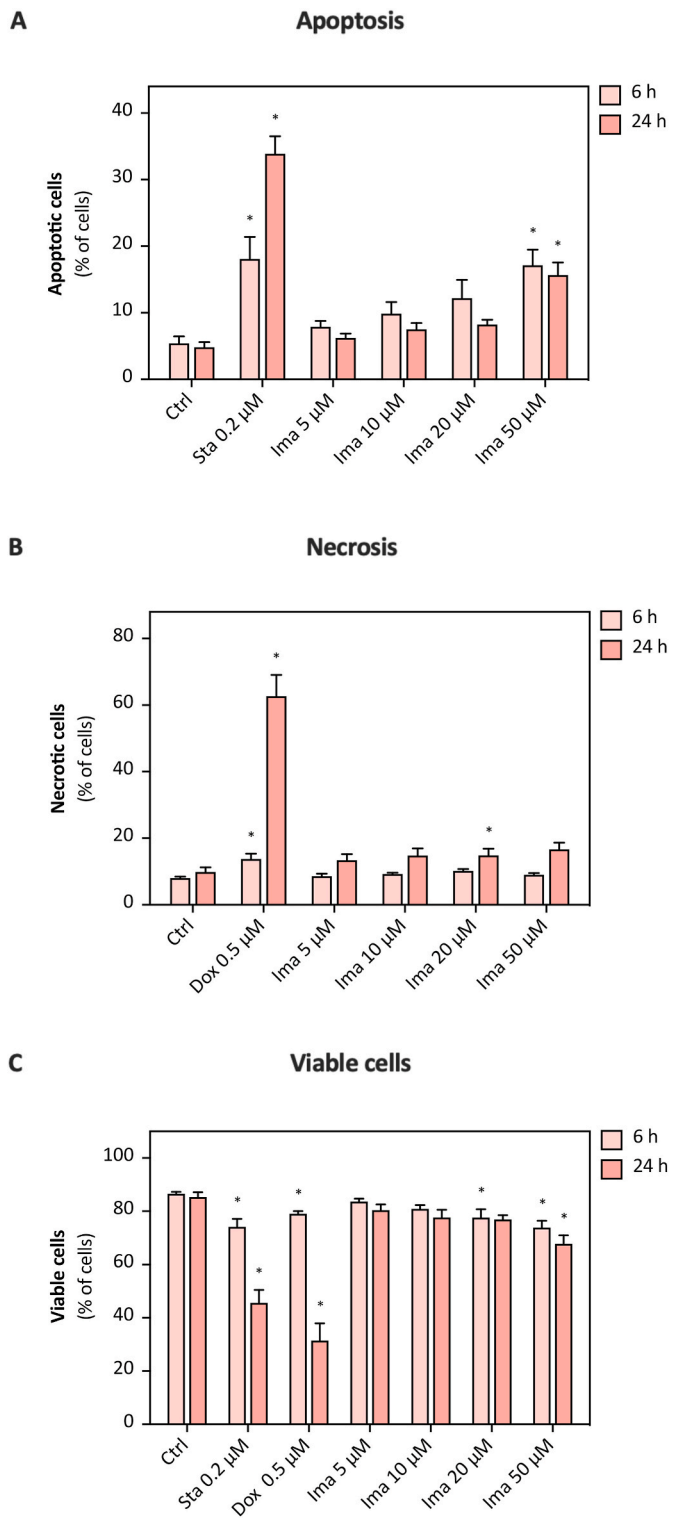

Fig. 8. Induction of apoptosis and necrosis. Percentage of (**A**) apoptotic, (**B**) necrotic and (**C**) viable HepG2 cells upon treatment with imatinib (5–50 μM) for 6 h and 24 h. Staurosporine (Sta) and doxorubicin (Dox) represent positive control for apoptosis and necrosis, respectively. The sum of apoptotic, necrotic, and viable cells was set as 100%. The percentage (%) of cells is shown as the mean ± SEM of four independent replicates. *$p < 0.05$ versus negative control. Ima: Imatinib.

(Morissette et al., 2009). Chloroquine, for instance, is a widely used late-stage inhibitor of autophagy (Klionsky et al., 2016). Ineffective autophagy can lead to lysosomal membrane permeabilization (LMP), which is associated with lysosome-dependent cell death (Galluzzi et al., 2018). LMP can induce both mitochondria-dependent and mitochondria-independent cell death through release of lysosomal proteases (i.e., cathepsins) into the cytoplasm (Aits and Jäättelä, 2013; Boya et al., 2003a). Cytosolic cathepsins that remain active at neutral pH (e.g., CTSB) can trigger mitochondrial membrane permeabilization, leading to cytochrome *c* release and induction of apoptosis (Aits and Jäättelä, 2013; Boya and Kroemer, 2008). In support of this notion, imatinib-induced LMP with subsequent activation and release of CTSB into the cytosol has been reported to contribute to the antileukemic effect of imatinib in CML cell models and CD34-positive cells from CML patients (Puissant et al., 2010).

We previously proposed mitochondrial dysfunction as a primary cause of imatinib-associated toxicity in HepG2 cells (Paech et al., 2017). Considering the results of the current study, lysosomal dysfunction appears to play at least an equally important role and may be the first step in the hepatotoxicity of imatinib and lapatinib. Lysosomal dysfunction impairs mitophagy, impeding the removal of damaged, potentially toxic mitochondria. Lysosomal dysfunction and ROS from damaged mitochondria can trigger LMP (Aits and Jäättelä, 2013), which stimulates apoptosis by causing mitochondrial membrane permeability transition and release of cytochrome *c* into the cytoplasm. The current study reveals the main toxicological mechanisms of lysosomotropic compounds and suggests a possible interplay with mitochondrial toxicity.

Conflict of interest

We declare that the research was conducted in the absence of any commercial or financial relationships that could be construed as a potential conflict of interest.

Funding

This research did not receive any specific grant from funding agencies in the public, commercial, or not-for-profit sectors.

CRediT authorship contribution statement

Noëmi Johanna Roos: conducted the experiments, interpreted data, prepared the figures, Writing – original draft. **Riccardo Vincenzo Mancuso:** conducted the experiments, interpreted data, prepared the figures, Writing – original draft. **Gerda Mawududzi Sanvee:** Methodology, interpreting data. **Jamal Bouitbir:** Methodology, interpreting data. **Stephan Krähenbühl:** Methodology, discussed and helped interpreting the data, Writing – original draft.

Declaration of competing interest

The authors declare that they have no known competing financial interests or personal relationships that could have appeared to influence the work reported in this paper.

Acknowledgement

We thank Cinzia Tiberi from the BioEM Lab of the Biozentrum, University of Basel, for her kind support with the transmission electron microscopy. We also thank Jens Casper from the Pharmaceutical Technology, University of Basel, for providing HuH-7 cells.

Appendix A. Supplementary data

Supplementary data to this article can be found online at https://doi.org/10.1016/j.fct.2022.112869.

References

Aits, S., Jäättelä, M., 2013. Lysosomal cell death at a glance. J. Cell Sci. 126, 1905–1912.

Azim Jr., H.A., et al., 2013. Pattern of rash, diarrhea, and hepatic toxicities secondary to lapatinib and their association with age and response to neoadjuvant therapy: analysis from the NeoALTTO trial. J. Clin. Oncol. 31, 4504–4511.

Boya, P., et al., 2003a. Lysosomal membrane permeabilization induces cell death in a mitochondrion-dependent fashion. J. Exp. Med. 197, 1323–1334.

Boya, P., et al., 2003b. Mitochondrial membrane permeabilization is a critical step of lysosome-initiated apoptosis induced by hydroxychloroquine. Oncogene 22, 3927–3936.

Boya, P., Kroemer, G., 2008. Lysosomal membrane permeabilization in cell death. Oncogene 27, 6434–6451.

Burger, H., et al., 2015. Lysosomal sequestration determines intracellular imatinib levels. Mol. Pharmacol. 88, 477–487.

Chu, Q.S., et al., 2007. Phase I and pharmacokinetic study of lapatinib in combination with capecitabine in patients with advanced solid malignancies. J. Clin. Oncol. 25, 3753–3758.

de Duve, C., et al., 1974. Commentary. Lysosomotropic agents. Biochem. Pharmacol. 23, 2495–2531.

Druker, B.J., et al., 2001. Efficacy and safety of a specific inhibitor of the BCR-ABL tyrosine kinase in chronic myeloid leukemia. N. Engl. J. Med. 344, 1031–1037.

Egan, D.F., et al., 2015. Small molecule inhibition of the autophagy kinase ULK1 and identification of ULK1 substrates. Mol. Cell 59, 285–297.

Ertmer, A., et al., 2007. The anticancer drug imatinib induces cellular autophagy. Leukemia 21, 936–942.

Fu, D., et al., 2014. Imaging the intracellular distribution of tyrosine kinase inhibitors in living cells with quantitative hyperspectral stimulated Raman scattering. Nat. Chem. 6, 614–622.

Funk, R.S., Krise, J.P., 2012. Cationic amphiphilic drugs cause a marked expansion of apparent lysosomal volume: implications for an intracellular distribution-based drug interaction. Mol. Pharm. 9, 1384–1395.

Galluzzi, L., et al., 2018. Molecular mechanisms of cell death: recommendations of the nomenclature committee on cell death 2018. Cell Death Differ. 25, 486–541.

Gardner, E.R., et al., 2009. Influence of the dual ABCB1 and ABCG2 inhibitor tariquidar on the disposition of oral imatinib in mice. J. Exp. Clin. Cancer Res. 28, 99.

Goldman, J.M., Melo, J.V., 2001. Targeting the BCR-ABL tyrosine kinase in chronic myeloid leukemia. N. Engl. J. Med. 344, 1084–1086.

Hara, T., et al., 2006. Suppression of basal autophagy in neural cells causes neurodegenerative disease in mice. Nature 441, 885–889.

Huang, L., et al., 2020. Tyrosine kinase inhibitors for solid tumors in the past 20 years (2001-2020). J. Hematol. Oncol. 13, 143.

Hudachek, S.F., Gustafson, D.L., 2013. Physiologically based pharmacokinetic model of lapatinib developed in mice and scaled to humans. J. Pharmacokinet. Pharmacodyn. 40, 157–176.

Kim, J., et al., 2011. AMPK and mTOR regulate autophagy through direct phosphorylation of Ulk1. Nat. Cell Biol. 13, 132–141.

Klionsky, D.J., et al., 2016. Guidelines for the use and interpretation of assays for monitoring autophagy. Autophagy 12, 1–222 third ed.

Kominami, E., et al., 1988. Biosyntheses and processing of lysosomal cysteine proteinases in rat macrophages. FEBS Lett. 231, 225–228.

Krause, D.S., Van Etten, R.A., 2005. Tyrosine kinases as targets for cancer therapy. N. Engl. J. Med. 353, 172–187.

Kwiatkowski, D.J., Manning, B.D., 2005. Tuberous sclerosis: a GAP at the crossroads of multiple signaling pathways. Hum. Mol. Genet. 14 (2), R251–R258.

Lin, N.U., et al., 2003. Fatal hepatic necrosis following imatinib mesylate therapy. Blood 102, 3455–3456.

Lu, S., et al., 2017. Lysosomal adaptation: how cells respond to lysosomotropic compounds. PLoS One 12, e0173771.

Morissette, G., et al., 2009. Intracellular sequestration of amiodarone: role of vacuolar ATPase and macroautophagic transition of the resulting vacuolar cytopathology. Br. J. Pharmacol. 157, 1531–1540.

Morissette, G., et al., 2008. Intense pseudotransport of a cationic drug mediated by vacuolar ATPase: procainamide-induced autophagic cell vacuolization. Toxicol. Appl. Pharmacol. 228, 364–377.

Moy, B., et al., 2007. Lapatinib. Nat. Rev. Drug Discov. 6, 431–432.

Nada, S., et al., 2009. The novel lipid raft adaptor p18 controls endosome dynamics by anchoring the MEK-ERK pathway to late endosomes. EMBO J. 28, 477–489.

Nadanaciva, S., et al., 2011. A high content screening assay for identifying lysosomotropic compounds. Toxicol. Vitro 25, 715–723.

Ostenfeld, M.S., et al., 2008. Anti-cancer agent siramesine is a lysosomotropic detergent that induces cytoprotective autophagosome accumulation. Autophagy 4, 487–499.

Paech, F., et al., 2017. Hepatocellular toxicity associated with tyrosine kinase inhibitors: mitochondrial damage and inhibition of glycolysis. Front. Pharmacol. 8, 367.

Paech, F., et al., 2018. Mechanisms of mitochondrial toxicity of the kinase inhibitors ponatinib, regorafenib and sorafenib in human hepatic HepG2 cells. Toxicology 395, 34–44.

Palmgren, M.G., 1991. Acridine orange as a probe for measuring pH gradients across membranes: mechanism and limitations. Anal. Biochem. 192, 316–321.

Peng, B., et al., 2005. Clinical pharmacokinetics of imatinib. Clin. Pharmacokinet. 44, 879–894.

Poole, B., Ohkuma, S., 1981. Effect of weak bases on the intralysosomal pH in mouse peritoneal macrophages. J. Cell Biol. 90, 665–669.

Puertollano, R., et al., 2018. The complex relationship between TFEB transcription factor phosphorylation and subcellular localization. EMBO J. 37.

Puissant, A., et al., 2010. Cathepsin B release after imatinib-mediated lysosomal membrane permeabilization triggers BCR-ABL cleavage and elimination of chronic myelogenous leukemia cells. Leukemia 24, 115–124.

Reis, R.C., et al., 1998. A novel methodology for the investigation of intracellular proteolytic processing in intact cells. Eur. J. Cell Biol. 75, 192–197.

Roczniak-Ferguson, A., et al., 2012. The transcription factor TFEB links mTORC1 signaling to transcriptional control of lysosome homeostasis. Sci. Signal. 5, ra42.

Roos, N.J., et al., 2020. The uricosuric benzbromarone disturbs the mitochondrial redox homeostasis and activates the NRF2 signaling pathway in HepG2 cells. Free Radic. Biol. Med. 152, 216–226.

Ryan, Q., et al., 2008. FDA drug approval summary: lapatinib in combination with capecitabine for previously treated metastatic breast cancer that overexpresses HER-2. Oncol. 13, 1114–1119.

Sancak, Y., et al., 2010. Ragulator-Rag complex targets mTORC1 to the lysosomal surface and is necessary for its activation by amino acids. Cell 141, 290–303.

Sanvee, G.M., et al., 2019. Insulin prevents and reverts simvastatin-induced toxicity in C2C12 skeletal muscle cells. Sci. Rep. 9, 7409.

Sardiello, M., et al., 2009. A gene network regulating lysosomal biogenesis and function. Science 325, 473–477.

Settembre, C., et al., 2011. TFEB links autophagy to lysosomal biogenesis. Science 332, 1429–1433.

Skoupa, N., et al., 2020. Lysosomal fusion: an efficient mechanism increasing their sequestration capacity for weak base drugs without apparent lysosomal biogenesis. Biomolecules 10.

Xu, H., Ren, D., 2015. Lysosomal physiology. Annu. Rev. Physiol. 77, 57–80.

Yoshimori, T., et al., 1991. Bafilomycin A1, a specific inhibitor of vacuolar-type H(+)-ATPase, inhibits acidification and protein degradation in lysosomes of cultured cells. J. Biol. Chem. 266, 17707–17712.

Zhitomirsky, B., et al., 2018. Lysosomotropic drugs activate TFEB via lysosomal membrane fluidization and consequent inhibition of mTORC1 activity. Cell Death Dis. 9, 1191.